Editors' Suggestion

Generation of Circulating Cavity Magnon Polaritons

Jeremy Bourhill,[1,*] Weichao Yu,[2,3] Vincent Vlaminck,[4,5] Gerrit E. W. Bauer,[6,7,8,9] Giuseppe Ruoso,[10] and Vincent Castel[4,5]

[1] *Quantum Technologies and Dark Matter Research Lab, Department of Physics, University of Western Australia, 35 Stirling Highway, Crawley, Western Australia 6009, Australia*

[2] *State Key Laboratory of Surface Physics and Institute for Nanoelectronic Devices and Quantum Computing, Fudan University, Shanghai 200433, People's Republic of China*

[3] *Zhangjiang Fudan International Innovation Center, Fudan University, Shanghai 201210, People's Republic of China*

[4] *IMT Atlantique, Technopole Brest-Iroise, CS 83818, Brest Cedex 3 29238, France*

[5] *Laboratoire des Sciences et Technologies de l'Information, de la Communication et de la Connaissance (UMR 6285), CNRS, Technopole Brest-Iroise, CS 83818, Brest Cedex 3 29238, France*

[6] *World Premier International Research Center Initiative (WPI)—Advanced Institute of Materials Research (AIMR) and Institute for Materials Research (IMR), Tohoku University, Sendai 980-8577, Japan*

[7] *Kavli Institute for Theoretical Sciences, University of the Chinese Academy of Sciences, Beijing 10090, People's Republic of China*

[8] *Zernike Institute for Advanced Materials, Groningen University, 9700 AB Groningen, Kingdom of the Netherlands*

[9] *Kavli Institute for Theoretical Sciences, University of the Chinese Academy of Sciences, Beijing 10090, People's Republic of China*

[10] *Istituto Nazionale di Fisica Nucleare (INFN) Laboratori Nazionali di Legnaro, Viale Dell'Università 2, Legnaro, Padova 35020, Italy*

(Received 30 August 2022; revised 14 November 2022; accepted 7 December 2022; published 10 January 2023)

We experimentally realize circularly polarized unidirectional cavity magnon polaritons in a torus-shaped microwave cavity loaded by a small magnetic sphere. At special positions, the clockwise and counterclockwise modes are circularly polarized, such that only one of them couples to the magnet, which breaks the mode degeneracy. We reveal the chiral nature of the spectral energy and angular-momentum flow by observing and modeling nonreciprocities of the microwave scattering matrix.

DOI: 10.1103/PhysRevApplied.19.014030

I. INTRODUCTION

The study of cavity magnonics has led to the discovery of new and interesting regimes of the coupling dynamics between photons and magnons. The field attracted initial attention due to the relative ease of achieving strong coupling, even at room temperature [1–3], because the large spin density in magnetic materials leads to a large coupling that easily exceeds cavity loss rates and thereby hybridized quasiparticles (magnon polaritons). Also attractive is the tunability of the magnetic resonance by an applied external dc magnetic field through the cavity modes.

Specially designed cavities [4,5] and larger magnetic samples [3,6] reach the ultrastrong coupling regime, in which the magnon-photon coupling rate is a sizable fraction of the system frequency. Dissipative coupling [7–9] of magnets in open or leaky waveguides strongly modifies the dynamics, e.g., causing resonance-level attraction. Multiple magnets inside a cavity, also called magnonic molecules [10–14], sustain delocalized collective modes by the real or virtual exchange of cavity photons.

The observed nonreciprocity in (open or closed) microwave cavities is interesting for applications, since nonreciprocal microwave components are essential elements in classical and possibly quantum communication systems [15–17]. An isolator is a diodelike device that blocks signal flow in one direction, thereby protecting a circuit from unintended reflections, e.g., isolating the transmitter from the receiver in a radar architecture [18,19], to shield qubits from their environment [20–22], or to investigate topological materials [23,24]. The nonreciprocity of guided microwave propagation induced by a magnetic load, discovered in the 1960s, has been implemented in resonance absorption isolators [25,26]. More recently, Yu *et al.* [27] have proposed generating nonreciprocity in a circular microwave cavity by breaking its time-reversal

*jeremy.bourhill@uwa.edu.au

symmetry (TRS) with magnetic loads with preferential clockwise versus counterclockwise spin and energy flows. The TRS breaking can be achieved by positioning magnets on special chiral lines in a microwave cavity on which the propagating photons are chiral [28,29], i.e., the sign of their circular polarization is locked to their linear momentum. This causes a strong direction-dependent coupling with the magnon excitations that can be controlled by applied magnetic fields.

Here, we experimentally demonstrate circularly polarized unidirectional magnon polaritons, thereby confirming theoretical predictions [27]. We place an yttrium iron garnet (YIG) sphere inside a newly machined torus-shaped cavity in special positions and tune the magnetic resonance to a transverse-electric (TE) cavity mode. We detect the coupling dynamics in the microwave scattering matrix as a function of an applied magnetic field. The experimental results agree with the simulations and the nonreciprocity of scattering parameters confirm the chiral nature of the hybrid modes.

The demonstration that the insertion of magnetic material into a waveguide or resonator leads to unidirectional mode propagation without significant losses suggests applications as microwave isolators or circulators for multiplexed communications at microwave frequencies [30,31], masers [32,33] and quantum manipulation systems [34,35].

II. SYSTEM

The torus-shaped microwave cavity shown in Fig. 1 is machined from high-purity aluminum in two parts (lid and base). The inner and outer radii R_1 (15 mm) and R_2 (30 mm) and the height h (6 mm) are chosen to match the model parameters in Ref. [27]. Rather than drive the cavity by electrical probes in the z axis [27], we place two magnetic loops around the radial axis at $\varphi = \pm 90^\circ$ that couple to the H_ϕ component of the cavity field as shown in Fig. 1. These probes do not measurably affect the frequency response or the rf field distribution. The second azimuthal harmonic of the TE mode of the torus cavity resonates at $f_c = 10.8$ GHz with a quality factor $Q = 775$, which corresponds to a bandwidth of $\kappa/2\pi = 14$ MHz.

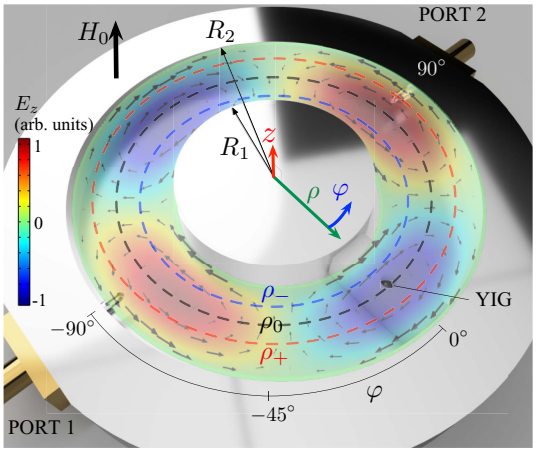

FIG. 1. A torus-shaped Al cavity overlaid with a snapshot of the simulated electromagnetic fields of the $m = 2$ TE cavity mode. The E_z amplitude is coded by the color density plot, while the arrow vector plot represents $\vec{H}$. The dashed lines indicate the special radial positions ρ_-, ρ_0, and ρ_+ (see the text). The YIG sphere in the sample holder is the black dot at $\rho = \rho_0$, $\varphi = 0$.

The pure single-crystal YIG sphere with a diameter of 1.8 mm is provided by the INFN Laboratori Nazionali di Legnaro. The grinding procedure [10] leads to a ferromagnetic resonance line width of approximately 4 MHz at 10 GHz. The magnon-photon coupling strength is mapped by putting the YIG sphere at different positions inside the cavity by means of a sample holder made from Rohacell® HF, with a hole drilled at the correct radial coordinates. All measurements are performed at room temperature. We align the external dc magnetic field H_0 along the easy axis of the magnetic sphere and the z axis of the cavity, i.e., $\langle 111 \rangle \parallel z$. Microwave spectra are recorded using a vector network analyzer at both ports as a function of the external dc magnetic field strength.

III. THEORY

The torus cavity is a rectangular waveguide [28,29] bent into a circle with specific azimuthal lines in the cavity at which the microwave magnetic field of the TE modes with $H_z = 0$ and $\partial_n E_z|_S = 0$ is circularly polarized [27]. Their radial positions follow from the analytic solution of Maxwell's equations in free space with perfect conducting boundary conditions at the metallic walls of the torus.

Due to the axial symmetry of the empty cavity, the field amplitudes are proportional to $e^{im\varphi}$, where m is an integer that labels the orbital angular momentum of clockwise (cw, $m > 0$) and counterclockwise (ccw, $m < 0$) photon circulation. Their linear combinations form phase-shifted standing waves with frequencies that may be split by a perturbation such as a YIG sphere.

The anticlockwise uniform precession of the magnetization (Kittel mode) around the effective magnetic field couples to photons with the same polarization [36]. Since we align the easy axis and H_0, a circularly polarized rf magnetic field couples to the Kittel mode only when right-hand circularly polarized ($|R\rangle$) with respect to the z axis. For a TE mode, $|R\rangle$ ($|L\rangle$) polarization corresponds to the relation $H_\varphi = iH_\rho$ ($H_\varphi = -iH_\rho$) between the polar components of the ac magnetic field. These conditions are fulfilled at specific radial locations $\rho_\pm$ for all m.

For a cw mode, the magnetic field has $|L\rangle$ polarization at ρ_- and $|R\rangle$ at ρ_+, and vice versa for a ccw mode. A sphere at these locations with magnetization along z couples to only one of these modes and breaks the degeneracy between them.

We define ρ_0 as the maximum of the linearly polarized E_z field, while $H_\varphi(\rho_0, \varphi) = 0$. Unlike $\rho_\pm$, the coupling along ρ_0 depends on the angle φ of the sphere position. The magnetic field is then linearly polarized with $H_\rho \propto \sin(m\varphi)$ and hence has maxima at $\varphi_1 = (n + 1/2)\pi/m$ and zeroes at $\varphi_2 = n\pi/m$ for $n = 0, 1, 2, \ldots$. At φ_1 for $\rho = \rho_0$, the cavity and Kittel modes maximally hybridize. The magnon-photon coupling is therefore chiral on $\rho = \rho_\pm$, not chiral and oscillating between zero and maxima as a function of φ at $\rho = \rho_0$, and partially chiral elsewhere [28].

We calculate the microwave-induced dynamics of the Kittel mode by solving the coupled Maxwell and linearized Landau-Lifshitz-Gilbert (LLG) equation in the frequency domain in the macrospin and rotating-wave approximations [13,37] using an electromagnetic finite-element solver in the frequency domain. We model the YIG sphere using a permittivity $\epsilon_r = 15$ [38] and a permeability μ_r that takes into account the external magnetic field and the frequency-dependent magnetic susceptibility:

$$\mu_r = \begin{pmatrix} 1+u & -iv & 0 \\ iv & 1+u & 0 \\ 0 & 0 & 1 \end{pmatrix}, \tag{1}$$

where $u = (\omega_K - i\alpha\omega)\omega_M/[(\omega_K - i\alpha\omega)^2 - \omega^2]$, $v = \omega\omega_M/[(\omega_K - i\alpha\omega)^2 - \omega^2]$, ω is the microwave frequency, $\omega_M = \gamma M_s$, $\omega_K = \gamma H_0$ the Kittel-mode frequency, γ is the gyromagnetic ratio, and α is the Gilbert damping constant. We can then calculate the observables, viz. the microwave transmission and reflection spectra, as measured by the two ports to the cavity [27].

We may infer the position-dependent coupling between the $m = 2$ TE cavity and the Kittel mode from the calculated transmission in Fig. 2 as a function of the microwave feed frequency and radial sphere position for two azimuthal angles. We observe all the qualitative features mentioned above, such as a vanishing coupling at the position ρ_0 in Fig. 2(a) compared to the anticrossing in Fig. 2(b). At $\rho_\pm$, the interaction splits two modes, rendering them all visible at any angle.

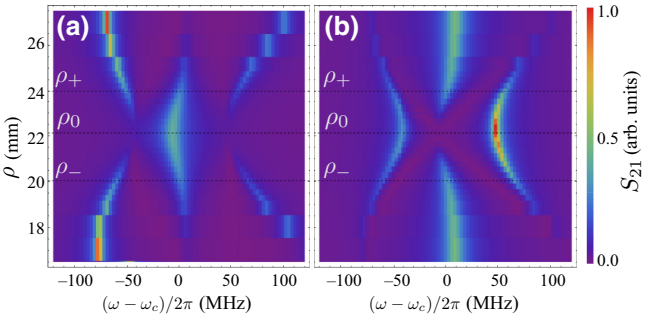

FIG. 2. Simulated microwave transmission amplitudes for the $m = 2$ TE mode of the torus cavity as a function of the radial sphere position along (a) $\varphi = 0°$ and (b) $\varphi = 45°$ and $H_0 = 0.3895$ T, tuned such that $\omega_m \approx \omega_c$. Special radial locations are marked by dashed lines.

The system can be accurately modeled by three coupled harmonic oscillators, viz. the two counter-rotating photonic modes and the magnetic mode. The second-quantized Hamiltonian reads

$$\begin{aligned} H_{\text{sys}} &= \hbar\omega_c a^\dagger a + \hbar\omega_c b^\dagger b + \hbar\omega_m m^\dagger m \\ &\quad + \hbar g_+(a^\dagger m + m^\dagger a) + \hbar g_-(b^\dagger m + m^\dagger b) \\ &\quad + \hbar J(a^\dagger b + b^\dagger a), \end{aligned} \tag{2}$$

where ω_c and ω_m are the cavity and magnon-mode frequencies, respectively, a, b, and m represent annihilation operators for the cw photonic mode, the ccw photonic mode, and the magnon mode, respectively, and the coupling between the respective photonic modes and the magnon, g_+ and g_-, depends on the position. J is a weak coupling between the two photonic modes by dielectric backscattering from the sphere or by the ports [39]. The action of J is to split the cavity mode into a doublet even far from the avoided crossing, which is observed experimentally [see Figs. 3(a) and 3(b)]. At very large H_0 values, the cavity mode will cease appearing as a doublet, but within the ω_m/ω_c range of Fig. 3, Eq. (2) is valid.

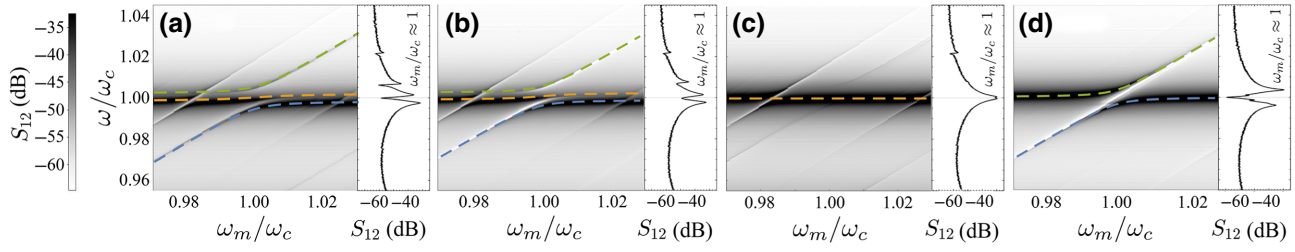

FIG. 3. Microwave transmission spectra $|S_{12}|$ close to the torus-cavity $m = 2$ TE mode ($\omega_c = 10.8$ GHz) and the Kittel mode of a 1.8-mm-diameter YIG sphere located at (a) $\{\varphi, \rho\} = \{0, \rho_-\}$, (b) $\{\varphi, \rho\} = \{0, \rho_+\}$, (c) $\{\varphi, \rho\} = \{0, \rho_0\}$, and (d) $\{\varphi, \rho\} = \{\pi/4, \rho_0\}$. The dashed lines are the eigenfrequency solutions of Eq. (2) with (a) $g_+ = 0$, (b) $g_- = 0$, and (c) $g_+ = g_- = J = 0$ and (d) is for a standard two coupled harmonic oscillator model. The panels on the right are line plots for the resonance $\omega_m/\omega_c \approx 1$.

Since the microwave field is circularly polarized at the special radial locations, $g_+(\rho_-,\varphi)=0$ and $g_-(\rho_+,\varphi)=0$ for $H_0>0$. g_+ and g_- can be expressed analytically [27] in the limit of small sphere radii and calculated numerically by the finite-element method [40].

At the special radii, our model splits into two separate systems: an uncoupled magnon mode and two coupled harmonic oscillators that form a magnon polariton. The amplitudes can be obtained by the standard input-output formalism for two ports [17,41] that leads to the 2×2 scattering matrix S. For example, the cw mode interacts with a sphere at ρ_+ when $H_0>0$ with scattering matrix

$$S = D_{\rm ccw}\left[-A_{\rm ccw}-i\omega I\right]^{-1}B_{\rm ccw} + \zeta D_{\rm cw}\left[-A_{\rm cw}-i\omega I\right]^{-1}B_{\rm cw}, \tag{3}$$

where

$$A_{\rm cw}=\begin{pmatrix}-i\omega_{\rm cw}-\frac{\kappa_0}{2} & ig\\ ig & -i\omega_m-\frac{\kappa_m}{2}\end{pmatrix},$$
$$B_{\rm cw}=\sqrt{\frac{\kappa_{\rm cw}}{2}}\begin{pmatrix}1 & e^{i\alpha_{\rm cw}}\\ 0 & 0\end{pmatrix},$$
$$A_{\rm ccw}=-i\omega_{\rm ccw}-\frac{\kappa_0}{2}, B_{\rm ccw}=\sqrt{\frac{\kappa_{\rm ccw}}{2}}\begin{pmatrix}1 & e^{i\alpha_{\rm ccw}}\end{pmatrix},$$
$$D_X=-CB_X^\dagger, C=\begin{pmatrix}\sqrt{1-\xi} & 1\sqrt{\xi}\\ i\sqrt{\xi} & \sqrt{1-\xi}\end{pmatrix},$$
$$\zeta=\begin{pmatrix}e^{i\beta} & 0\\ 0 & e^{-i\beta}\end{pmatrix}. \tag{4}$$

Here, $\omega_{\rm ccw/cw}$ are the mode frequencies, κ_0 is the cavity loss rate, $\kappa_{\rm cw/ccw}$ are the coupling loss rates, assumed equal at ports 1 and 2, $\alpha_{\rm cw/ccw}$ the phase difference between a mode excited at port 1 or port 2, and $0\le\xi\le 1$ represents the crosstalk between the two ports, and we assume that $\xi=0$, meaning no crosstalk. Since the cavity field at different positions is always in phase for standing waves, we have $\alpha_X=0$ [41]. We assume that a weak mode coupling J in Eq. (2) can be handled by slight shifts of the otherwise degenerate $\omega_{\rm cw/ccw}$ on the order of 20 MHz. β is the propagation phase difference between the two modes that are out-coupled through the same port. This phase factor depends on the flow direction, because a cw signal from port 2 first travels through the lower arm of the cavity with the YIG sample, while that from port 1 first has to travel through the upper arm before passing at port 2 and arriving at the YIG sphere because of the unidirectional nature of the propagating signals introduced by the YIG sphere, which is most prominent when on special lines $\rho_\pm$. In a partially open cavity, these phase differences lead to signatures of the unidirectional circulation of microwaves in the form of nonreciprocal transmission $S_{12}\neq S_{21}$. The couplings $\kappa_{\rm cw/ccw}$ may not be too small; when the photon lifetime in the cavity is long, the phase accumulated between the port and the magnet insertion does not play a role and the transmission is always reciprocal.

When $\omega_m\approx\omega_c$, the YIG sphere is at a chiral position, and the magnon-photon coupling is much larger than the backscattering J; the transmission spectra are characterized by a single magnon polariton with two resonances (peaks) at the eigenfrequencies of the hybrid system and an antiresonance (dip) at the uncoupled frequency [42,43] and a noninteracting cavity mode. Only the first term in Eq. (3) depends on the magnetic field and can lead to nonreciprocity.

We compare the calculated results with the experiments in Sec. IV, where appropriate.

IV. EXPERIMENTAL RESULTS

Figure 3 summarizes the microwave transmission spectra S_{21} for a 1.8-mm-diameter YIG sphere located at different positions within the torus close to the resonance $\omega_m=\omega_c$. We clearly observe the expected features owing to a magnon polariton when placing the YIG sphere on ρ_+ and ρ_-. On the other hand, the coupling nearly vanishes at ρ_0 and $\varphi=0^\circ$ and changes into a two-mode avoided level crossing for $\varphi=45^\circ$ as predicted [27].

Since the coupling is strong, we can directly read off the cavity-magnon coupling rates $g_\pm/2\pi$ in Eq. (2) from the experimental data. The dashed lines in Fig. 3 are eigenfrequencies of Eq. (2) with $g_X/2\pi=63$, 48, and 40 MHz for $\{\varphi,\rho\}=\{0^\circ,\rho_-\}$, $\{\varphi,\rho\}=\{0^\circ,\rho_+\}$, and $\{\varphi,\rho\}=\{45^\circ,\rho_0\}$, respectively. We deduce a much smaller $g_X/2\pi\approx 8.5$ MHz for $\{0^\circ,\rho_0\}$ from the splitting of the line plot of the S_{12} transmission spectra for $\omega_m=\omega_c$ in the right panel of Fig. 3(c).

Figure 4 shows the measured coupling rates between the 1.8-mm-diameter YIG sphere and the $m=2$ TE mode for $\varphi=0$, (red dots) and $\pi/4$ (red square) together with theory and simulations. The stars represent g as calculated by finite-element modeling, while the blue and yellow lines are analytical results for $g_{\pm m}$, respectively [27]. The theory and experiments, as well as $|g_{-m}-g_m|$ (green line) of the analytic and numerical results, agree very well. In the regions $\rho_-<\rho<\rho_+$, the contributions of cw and ccw waves to the coupling partly cancel, but they enhance each other otherwise.

A higher-order magnetostatic mode [44] in Fig. 3 appears under the main $\omega_m=\gamma H_0$ line (Kittel mode). It becomes observable by the nonuniformity of the magnetic field, which is larger along $\varphi=0^\circ$ as compared to $\varphi=45^\circ$, as seen by inspection of Fig. 1. This explains the observed stronger coupling of the higher spin wave for $\varphi=0^\circ$, i.e., Figs. 3(a)–3(c) versus Fig. 3(d). The higher-order (Walker) modes remain observable even when the sphere is at $\{0,\rho_0\}$ because of its finite size, which samples ac magnetic field gradients. The main higher-order

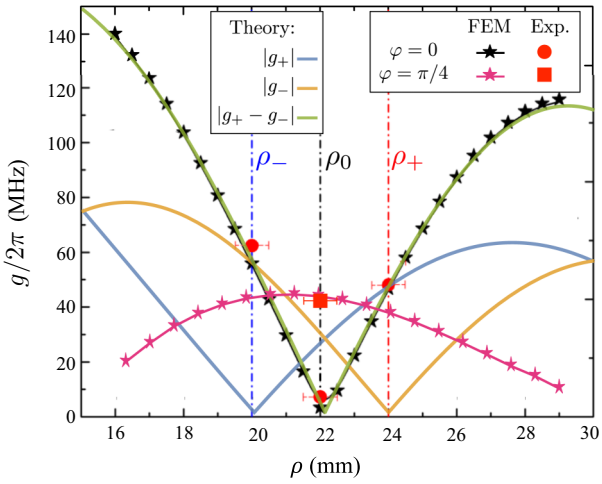

FIG. 4. The calculated (stars) and measured (red dots and square) magnon-photon coupling rates with the Kittel mode as a function of the radial position ρ along $\varphi = 0$ and $\varphi = \pi/4$. The special positions ρ_-, ρ_0 and ρ_+ are shown as blue, black, and red dashed lines, respectively.

mode is the same at all ρ at $\omega/\omega_c \approx 1.02$ in Fig. 3. Crossing the cavity frequency at $\omega_m = 0.98\omega_c$, it is most likely the {200} magnetostatic mode [44] and it appears to be well described by a weaker two-level avoided crossing, but without the angular-momentum selection rules that govern the Kittel-mode resonance.

A strongly coupled ferromagnetic resonance with a cavity mode generates two hybrid modes. When crossing the resonances with increasing frequency, the transmission amplitude suffers a $-\pi$ phase shift. The antiresonance in the avoided-crossing gap is characterized by a dip in the transmission amplitude and a $+\pi$ phase shift [42,43]. The unperturbed magnetic mode frequency of an uncoupled cavity mode, on the other hand, causes a single amplitude peak and a pair of $(\pi, -\pi)$ phase shifts. The spectra in Figs. 5(a)–5(d), in which the spheres are on the two chiral lines, show significant nonreciprocities but approximately obey the symmetry relation $S_{12}(\rho_+) = S_{21}(\rho_-)$ and vice versa (this symmetry is not exact, because the couplings are not exactly the same). Alternatively, a reversal of the external magnetic field will have the same result (not shown). The significant $S_{12}(\rho_\pm) \neq S_{21}(\rho_\pm)$ is a strong evidence of chiral microwave energy flow that is rendered observable by the breaking of the up-down mirror symmetry by the load. When the magnet is placed on a nonchiral position at $\{\pi/4, \rho_0\}$, we recover a response as seen in conventional cavities [see Figs. 5(e) and 5(f)]. As expected, we do not observe a significant nonreciprocity in this case.

The action of the backscattering term J in Eq. (2) is to couple the noninteracting mode to the interacting mode. Therefore, the large shift in mode frequency caused by the magnon interacting with the latter creates a smaller knock-on effect in the former, as can be seen by the slight

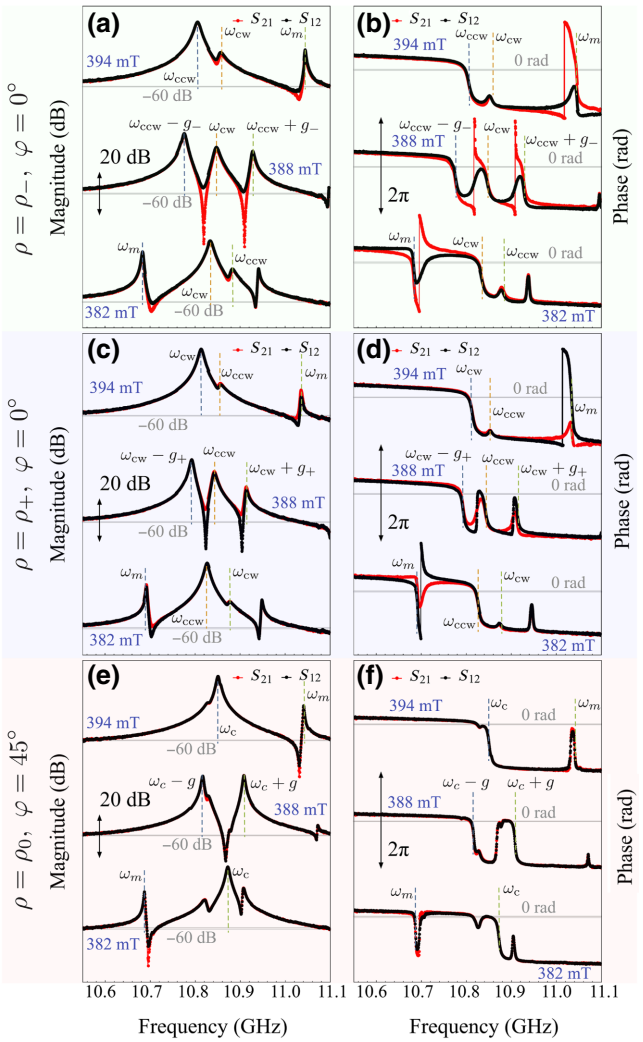

FIG. 5. The measured modulus (left) and phase (right) of the transmission amplitudes through a torus cavity with two ports in both directions, S_{21} (red line) and S_{12} (black line), loaded by a YIG sphere at ρ_- (top), ρ_+ (middle) and ρ_0, $\varphi = \pi/4$ as a function of the applied magnetic field.

perturbation of the yellow line in Figs. 3(a) and 3(b). This is a detail that is lost in the simplified approximate model of Eq. (3), which accounts for this effect by defining two mode frequencies independent of one another, which will be individually dependent on the applied magnetic field. This is why the frequencies $\omega_{\mathrm{cw/ccw}}$ are observed to shift as a function of H_0 in Fig. 5.

While the presence of J complicates the analysis, we can use the simplified Eq. (3) at the avoided crossing when $\omega_m \approx \omega_{\mathrm{ccw}}$ and $|g| \gg |J|$ to fit the scattering amplitude for the sphere at ρ_+ (for ρ_-, we have to change the roles of the cw and ccw modes). We can use independently observed values of $H = 0.3895$ T, $\kappa_0/2\pi = 14$ MHz, $\kappa_m/2\pi = 3.937$ MHz, $g/2\pi = 63$ MHz for ρ_-, and $g/2\pi = 48$ MHz for ρ_+ and set $\alpha_{\mathrm{cw}} = \alpha_{\mathrm{ccw}} = 0$. The external-port coupling rates $\kappa_{\mathrm{cw/ccw}}$, β, and $\omega_{\mathrm{cw/ccw}}$ are

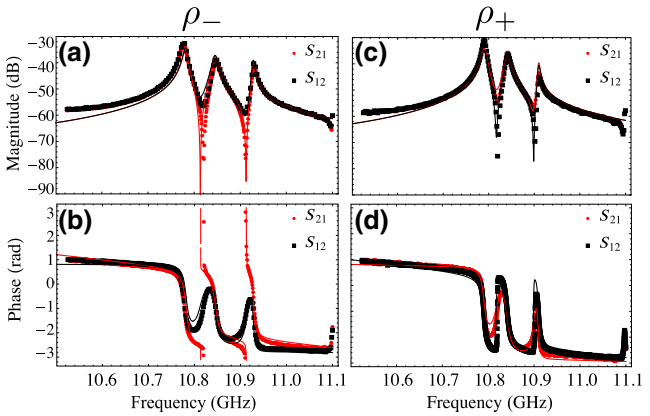

FIG. 6. Transmission spectra from Figs. 5(a)–5(d) for $\omega_m \approx \omega_c$ when the YIG sphere is located at ρ_- and ρ_+. The thin red and black lines are the fit obtained by the model scattering matrix (3).

fitting parameters. We model the resonance phase shift $\beta = B\ \mathrm{Erf}[(\omega - \omega_c)/\kappa_0]$ with $B \approx -0.4$, which fits the results for both ρ_+ and ρ_-, with the other parameters set to $\omega_{\mathrm{cw}}/2\pi = 10.818$ GHz, $\omega_{\mathrm{ccw}}/2\pi = 10.845$ GHz, $\kappa_{\mathrm{cw}} = 0.077\kappa_0$, and $\kappa_{\mathrm{ccw}} = 0.027\kappa_0$ for the sphere located at ρ_+. The ρ_- case can be modeled by swapping cw terms with ccw terms in Eq. (3) and changing the sign of B, because the transmission paths S_{21} and S_{12} have effectively been swapped. Hence given that all the other parameters are equal in amplitude, the difference in the phase shifts observable for the two radial positions is caused by the slightly stronger coupling at ρ_- [27]. Figure 6 shows excellent agreement of the model with experiments for both spectral features and the nonreciprocity.

We confirm the unidirectionality of the energy and angular-momentum flow in another torus-shaped cavity with three ports located symmetrically at angles of 120°, as shown in Fig. 7(a). Using port 2 (P_2) as input, unidirectionality should lead to different outputs at P_3 and P_1. The phases of $S_{32}$and S_{12} in Fig. 7(c) for $\omega_m < \omega_c$ and $\omega_m > \omega_c$ are very different when the sphere is located at ρ_+.

The phase shifts are associated with the different "arms" [17], i.e., the blue (upper) and green (lower) curves in Fig. 3(a). When the magnon is tuned below the cavity frequency, we see in Fig. 7(c) that a large phase shift is associated with the lower-frequency magnon-polariton signal S_{12} via the lower arm, while S_{32} is associated with the higher-frequency hybrid mode close to the cavity frequency via the upper arm. When $\omega_m > \omega_c$, the larger phase of S_{12} is locked to the cavity frequency but S_{32} follows ω_m. The two branches therefore maintain their phase shifts.

Figure 7(b) shows the simulated time evolution of the three eigenmodes when the YIG sphere is at ρ_+ and $\omega_m = \omega_c$. We see that the magnon-polariton modes have a cw ($m > 0$) orbital angular momentum, while the central noninteracting mode moves in the opposite direction ($m < 0$), as expected.

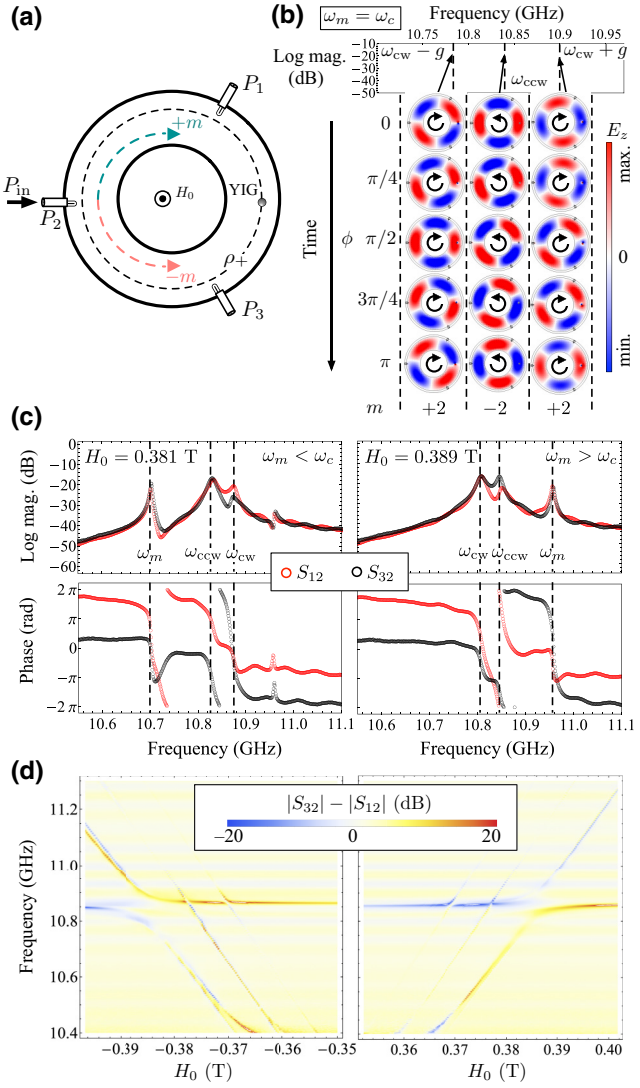

FIG. 7. (a) A schematic of the three-port microwave cavity and the position ρ_+ of the magnetic sample. (b) The time evolution of the phase (ϕ) of the eigenmodes calculated at $\omega_m = \omega_c$. The upper panel shows $|S_{12}|$ in red and $|S_{32}|$ in black. The lower panel contains snapshots of the electric field distribution E_z at the peaks of $|S_{xx}|$ (ω) that we associate with the magnon polariton (left and right, $m = +2$) and the noninteracting mode (center, $m = -2$) . We clearly observe the counter-rotation of the modes and the associated energy and angular-momentum flow as a function of the microwave frequency. (c) The experimental transmission amplitude with the modulus (top) and the phase (bottom) in the three-port setup for the sphere located at ρ_+, for $\omega_m < \omega_c$ (left) and $\omega_m > \omega_c$ (right). (d) The difference between the output in ports 1 $|S_{12}|$ and 3 $|S_{32}|$ when fed via port 2.

The asymmetry between the S_{12} and S_{32} phases is further direct evidence of unidirectionality, since it implies that the sphere is not at an equivalent position relative to the input and output probes. The difference in transmission amplitudes $|S_{32}| - |S_{12}|$ between the two output ports in Fig. 7(d) for $H_0 < 0$ and $H_0 > 0$ shows that the upper

branch has a higher transmission amplitude to P_1, while P_3 sees a larger amplitude for the lower branch. This situation is reversed with the magnetic field direction. The Kittel mode then precesses in the opposite direction, coupling to ccw modes with $|L\rangle$ polarization. Moving the sphere from ρ_+ to ρ_- while keeping H_0 fixed has a similar effect (not shown).

V. DISCUSSION

The spontaneous breaking of time-reversal symmetry is a unique feature of magnets that affects the interaction with electromagnetic radiation. In microwave guides and cavities, it enables a chiral magnon-photon coupling because the polarization of the electromagnetic radiation metallic boundaries is locked to its orbital motion on "chiral" lines or planes: a magnet placed at these special lines breaks the degeneracy of counterpropagating waves and results in unidirectional coupling.

Our observation of nonreciprocity in the scattering matrices of both two- and three-port torus cavities is direct proof of microwave circulation, i.e., the unidirectional nature of the magnon-polariton modes over macroscopic distances, which is induced by a relatively very small magnetic load. The experimental results agree very well with finite-difference calculations of the coupled Landau-Lifshitz and Maxwell equations and can be understood by a three-mode input-output model [27]. The direction of the microwave circulation can be reversed by tuning the frequency, flipping the magnetization direction, or shifting the position of the magnet. We may also envision multiple magnets placed on the same special line, which can be excited into resonance by local coils. Such a device can generate a high-power unidirectional photon beam with high coherence and narrow bandwidth.

ACKNOWLEDGMENTS

This work was funded by the Région Bretagne through the project OSCAR-SAD18024. This work is also part of the research program supported by the European Union through the European Regional Development Fund (ERDF) and by the Ministry of Higher Education and Research, Brittany and Rennes Mé tropole through the contrats de plan État-Région (CPER) Project Contrat de plan État-Région SOPHIE (STIC & Ondes Photonique). J.B. is supported by the Australian Research Council Centre of Excellence for Engineered Quantum Systems, CE170100009 and the Centre of Excellence for Dark Matter Particle Physics, CE200100008. W.Y. is supported by the Shanghai Pujiang Program (No. 21PJ1401500) and the Shanghai Science and Technology Committee (No. 21JC1406200) and G.B. by the Japan Society for the Promotion of Science (JSPS) KAKENHI Grant No. 19H00645.

[1] Y. Tabuchi, S. Ishino, T. Ishikawa, R. Yamazaki, K. Usami, and Y. Nakamura, Hybridizing Ferromagnetic Magnons and Microwave Photons in the Quantum Limit, Phys. Rev. Lett. **113**, 083603 (2014).

[2] H. Huebl, C. W. Zollitsch, J. Lotze, F. Hocke, M. Greifenstein, A. Marx, R. Gross, and S. T. B. Goennenwein, High Cooperativity in Coupled Microwave Resonator Ferrimagnetic Insulator Hybrids, Phys. Rev. Lett. **111**, 127003 (2013).

[3] X. Zhang, C.-L. Zou, L. Jiang, and H. X. Tang, Strongly Coupled Magnons and Cavity Microwave Photons, Phys. Rev. Lett. **113**, 156401 (2014).

[4] M. Goryachev, W. G. Farr, D. L. Creedon, Y. Fan, M. Kostylev, and M. E. Tobar, High-Cooperativity Cavity QED with Magnons at Microwave Frequencies, Phys. Rev. Appl. **2**, 054002 (2014).

[5] G. Flower, M. Goryachev, J. Bourhill, and M. E. Tobar, Experimental implementations of cavity-magnon systems: From ultra strong coupling to applications in precision measurement, New J. Phys. **21**, 095004 (2019).

[6] J. Bourhill, N. Kostylev, M. Goryachev, D. L. Creedon, and M. E. Tobar, Ultrahigh cooperativity interactions between magnons and resonant photons in a YIG sphere, Phys. Rev. B **93**, 144420 (2016).

[7] M. Harder, Y. Yang, B. M. Yao, C. H. Yu, J. W. Rao, Y. S. Gui, R. L. Stamps, and C.-M. Hu, Level Attraction Due to Dissipative Magnon-Photon Coupling, Phys. Rev. Lett. **121**, 137203 (2018).

[8] D. Zhang, X.-Q. Luo, Y.-P. Wang, T.-F. Li, and J. Q. You, Observation of the exceptional point in cavity magnon-polaritons, Nat. Commun. **8**, 1368 (2017).

[9] J. W. Rao, P. C. Xu, Y. S. Gui, Y. P. Wang, Y. Yang, B. Yao, J. Dietrich, G. E. Bridges, X. L. Fan, D. S. Xue, and C. M. Hu, Interferometric control of magnon-induced nearly perfect absorption in cavity magnonics, Nat. Commun. **12**, 1933 (2021).

[10] N. Crescini, C. Braggio, G. Carugno, A. Ortolan, and G. Ruoso, Coherent coupling between multiple ferrimagnetic spheres and a microwave cavity in the quantum-limit (2020), ArXiv:2007.08908.

[11] N. J. Lambert, J. A. Haigh, S. Langenfeld, A. C. Doherty, and A. J. Ferguson, Cavity-mediated coherent coupling of magnetic moments, Phys. Rev. A **93**, 021803 (2016).

[12] P.-C. Xu, J. W. Rao, Y. S. Gui, X. Jin, and C.-M. Hu, Cavity-mediated dissipative coupling of distant magnetic moments: Theory and experiment, Phys. Rev. B **100**, 094415 (2019).

[13] B. Z. Rameshti and G. E. W. Bauer, Indirect coupling of magnons by cavity photons, Phys. Rev. B **97**, 014419 (2018).

[14] X. Zhang, C.-L. Zou, N. Zhu, F. Marquardt, L. Jiang, and H. X. Tang, Magnon dark modes and gradient memory, Nat. Commun. **6**, 8914 (2015).

[15] N. Zhu, X. Han, C.-L. Zou, M. Xu, and H. X. Tang, Magnon-photon strong coupling for tunable microwave circulators, Phys. Rev. A **101**, 043842 (2020).

[16] C. Caloz, A. Alù, S. Tretyakov, D. Sounas, K. Achouri, and Z.-L. Deck-Léger, Electromagnetic Nonreciprocity, Phys. Rev. Appl. **10**, 047001 (2018).

[17] Y. Shi, C. Zhang, C. Jiang, C. K. Ong, and G. Chai, Mirror symmetric nonreciprocity and circular transmission

in cavity magnonics, Appl. Phys. Lett. **119**, 132403 (2021).
[18] M. Mahdi, M. Darwish, H. Tork, and A. El-Tager, An improved self-interference canceller for X-band radar transceivers, IET Microwaves, Antennas Propag. **15**, 1381 (2021).
[19] Z. Li and K. Wu, in *2008 Global Symposium on Millimeter Waves* (2008), p. 127.
[20] B. Abdo, N. T. Bronn, O. Jinka, S. Olivadese, A. D. Córcoles, V. P. Adiga, M. Brink, R. E. Lake, X. Wu, D. P. Pappas, and J. M. Chow, Active protection of a superconducting qubit with an interferometric josephson isolator, Nat. Commun. **10**, 3154 (2019).
[21] R. Vijay, D. H. Slichter, and I. Siddiqi, Observation of Quantum Jumps in a Superconducting Artificial Atom, Phys. Rev. Lett. **106**, 110502 (2011).
[22] M. Hatridge, S. Shankar, M. Mirrahimi, F. Schackert, K. Geerlings, T. Brecht, K. M. Sliwa, B. Abdo, L. Frunzio, S. M. Girvin, R. J. Schoelkopf, and M. H. Devoret, Quantum back-action of an individual variable-strength measurement, Science **339**, 178 (2013).
[23] T. Huang, L. Li, J. Li, X. Zhu, P. Lan, and P. Lu, Polarization-resolved analysis to solid high-order harmonic generation, J. Phys. B: At., Mol. Opt. Phys. **55**, 095601 (2022).
[24] S. A. O. Motlagh, F. Nematollahi, V. Apalkov, and M. I. Stockman, Topological resonance and single-optical-cycle valley polarization in gapped graphene, Phys. Rev. B **100**, 115431 (2019).
[25] A. J. B. Fuller, and Institution of Electrical Engineers, *Ferrites at Microwave Frequencies*, IEE Electromagnetic Waves Series (P. Peregrinus, 1987).
[26] E. Schlomann, On the theory of the ferrite resonance isolator, IRE Trans. Microwave Theory Tech. **8**, 199 (1960).
[27] W. Yu, T. Yu, and G. E. W. Bauer, Circulating cavity magnon polaritons, Phys. Rev. B **102**, 064416 (2020).
[28] T. Yu, X. Zhang, S. Sharma, Y. M. Blanter, and G. E. W. Bauer, Chiral coupling of magnons in waveguides, Phys. Rev. B **101**, 094414 (2020).
[29] T. Yu, Y.-X. Zhang, S. Sharma, X. Zhang, Y. M. Blanter, and G. E. W. Bauer, Magnon Accumulation in Chirally Coupled Magnets, Phys. Rev. Lett. **124**, 107202 (2020).
[30] W. Zhang, S. Zheng, X. Hui, R. Dong, X. Jin, H. Chi, and X. Zhang, Mode division multiplexing communication using microwave orbital angular momentum: An experimental study, IEEE Trans. Wireless Commun. **16**, 1308 (2017).
[31] X. Zeng, P. St. J. Russell, C. Wolff, M. H. Frosz, G. K. L. Wong, and B. Stiller, Nonreciprocal vortex isolator via topology-selective stimulated Brillouin scattering, Sci. Adv. **8**, eabq6064 (2022).
[32] J. E. Geusic and H. E. D. Scovil, A unidirectional traveling-wave optical maser, The Bell Syst. Tech. J. **41**, 1371 (1962).
[33] J. Bourhill, K. Benmessai, M. Goryachev, D. L. Creedon, W. Farr, and M. E. Tobar, Spin bath maser in a cryogenically cooled sapphire whispering gallery mode resonator, Phys. Rev. B **88**, 235104 (2013).
[34] T. Liu, X. Zhu, F. Chen, S. Liang, and J. Zhu, Unidirectional Wave Vector Manipulation in Two-Dimensional Space with an All Passive Acoustic Parity-Time-Symmetric Metamaterials Crystal, Phys. Rev. Lett. **120**, 124502 (2018).
[35] G. Vallone, E. Pomarico, F. De Martini, and P. Mataloni, One-way quantum computation via manipulation of polarization and momentum qubits in two-photon cluster states, Laser Phys. Lett. **5**, 398 (2008).
[36] Y. Nambu, J. Barker, Y. Okino, T. Kikkawa, Y. Shiomi, M. Enderle, T. Weber, B. Winn, M. Graves-Brook, J. M. Tranquada, T. Ziman, M. Fujita, G. E. W. Bauer, E. Saitoh, and K. Kakurai, Observation of Magnon Polarization, Phys. Rev. Lett. **125**, 027201 (2020).
[37] Y. Cao, P. Yan, H. Huebl, S. T. B. Goennenwein, and G. E. W. Bauer, Exchange magnon-polaritons in microwave cavities, Phys. Rev. B **91**, 094423 (2015).
[38] K. Sadhana, R. S. Shinde, and S. R. Murthy, Synthesis of nanocrystalline YIG using microwave-hydrothermal method, Int. J. Mod. Phys. B **23**, 3637 (2009).
[39] M. Goryachev, W. G. Farr, D. L. Creedon, and M. E. Tobar, Spin-photon interaction in a cavity with time-reversal symmetry breaking, Phys. Rev. B **89**, 224407 (2014).
[40] J. Bourhill, V. Castel, A. Manchec, and G. Cochet, Universal characterization of cavity-magnon polariton coupling strength verified in modifiable microwave cavity, J. Appl. Phys. **128**, 073904 (2020).
[41] X. Zhang, A. Galda, X. Han, D. Jin, and V. M. Vinokur, Broadband Nonreciprocity Enabled by Strong Coupling of Magnons and Microwave Photons, Phys. Rev. Appl. **13**, 044039 (2020).
[42] M. Harder and C.-M. Hu, Chapter two—cavity spintronics: An early review of recent progress in the study of magnon-photon level repulsion, Solid State Phys. **69**, 47 (2018).
[43] M. Harder, P. Hyde, L. Bai, C. Match, and C.-M. Hu, Spin dynamical phase and antiresonance in a strongly coupled magnon-photon system, Phys. Rev. B **94**, 054403 (2016).
[44] J. A. Haigh, N. J. Lambert, S. Sharma, Y. M. Blanter, G. E. W. Bauer, and A. J. Ramsay, Selection rules for cavity-enhanced Brillouin light scattering from magnetostatic modes, Phys. Rev. B **97**, 214423 (2018).